Theoretical simulation of holographic polymer-dispersed liquid-crystal films via pattern photopolymerization-induced phase separation

Thein Kyu,* Domasius Nwabunma,† and Hao-Wen Chiu‡
Institute of Polymer Engineering, The University of Akron, Akron, Ohio 44325
(Received 13 July 2000; published 15 May 2001)

A theoretical simulation has been performed to elucidate the emergence of nematic domains during pattern photopolymerization-induced phase separation in holographic polymer-dispersed liquid crystals. We consider a reference system consisting of a single-component nematic, namely, 4-*n*-heptyl-4′-cyanobiphenyl (T_{NI} = 42 °C), and a polymer network made from multifunctional monomers. To mimic pattern photopolymerization, the reaction rate was varied periodically in space through wave mixing. In the theoretical development, the photopolymerization kinetics was coupled with the time-dependent Ginzburg-Landau model *C* equations by incorporating the local free energy densities pertaining to isotropic liquid-liquid mixing, nematic ordering, and network elasticity. The simulated morphological patterns in the concentration and orientation order parameter fields show discrete layers of liquid-crystal droplets alternating periodically with polymer-network-rich layers. The Fourier transforms of these patterns show sharp diffraction spots arising from the periodic layers. As the layer thickness is reduced, the liquid-crystal molecules are confined in the narrow stripes. The liquid-crystal domains appear uniform along the stripes, which in turn gives rise to sharper diffraction spots in Fourier space. Of particular interest is that our simulated stratified patterns are in qualitative agreement with reported experimental observations.

DOI: 10.1103/PhysRevE.63.061802 PACS number(s): 61.25.Hq, 61.41.+e, 64.75.+g

I. INTRODUCTION

It has been well established that thin composite films containing liquid crystals (LC's) and polymers are heterogeneous systems generally prepared via phase separation induced by thermal quenching, solvent removal, and thermally or photochemically initiated polymerization [1,2]. Of these methods, polymerization-induced phase separation (PIPS) initiated by UV radiation is a preferred way of producing these composite films because of the ease of the fabrication process, which requires no solvent. Polymer-dispersed liquid crystals (PDLC's) containing substantial amounts of polymer and polymer-stabilized liquid crystals (PSLC's) containing a very small amount of network polymer are two common types of LC/polymer composite. These composites have been customarily prepared via PIPS under uniform UV irradiation to obtain uniform distributions of LC droplets in a continuum of cross-linked polymer.

Recently, another type of LC/polymer composite known as a holographic polymer-dispersed liquid crystal (H-PDLC) composite has been developed [3–8] through pattern photopolymerization-induced phase separation of LC/monomer mixtures by wave mixing, viz., allowing two propagating UV laser beams to interfere at a certain angle. The constructive and destructive interference of these planar waves gives rise to stripe fringes, the periodicity of which depends on the incident angles. When the spatially modulated UV intensity fringes are imprinted on LC/photoreactive-monomer mixtures, photoreaction takes place in periodic striations, thereby creating a H-PDLC film with alternating LC-rich and polymer-rich layers. The refractive index mismatch between the H-PDLC layers gives rise to diffraction of light, while the LC directors can be electrically switched across the film. Thus H-PDLC's have found potential applications such as spatial light modulators, agile filters, beam steering, etc.

Most studies on H-PDLC films hitherto reported have focused on experimental investigations of the effects of monomer type, functionality, and LC concentration on morphology development and electro-optical properties [3–8]. For efficient fabrication of H-PDLC's, it is essential to better understand the mechanism underlying the pattern forming process. Krongauz, Schmelzer, and Yohannan [9] studied the kinetics of anisotropic photopolymerization in a plasticized polymer without examining any phase separation or mesophase ordering. On the other hand, Wang, Yu, and Taylor [10] performed a one-dimensional simulation on anisotropic phase separation in a PDLC system based on the Monte Carlo approach. Although the qualitative features of the H-PDLC structure were captured in the simulation, the nematic ordering of the LC directors was not accounted for in their theoretical formulation.

In this paper, we undertake a two-dimensional simulation of a H-PDLC via stratified pattern photopolymerization-induced phase separation by incorporating the pertinent photopolymerization kinetics. In the simulation, we employ some material parameters such as the nematic-isotropic transition temperature of the LC, network functionality, etc., of a reference system that has been studied extensively in our laboratory [11–13]. The spatiotemporal evolution of the concentration and orientational order parameters has been calcu-

*Author to whom correspondence should be addressed. Email address: tkyu@uakron.edu
†Present address: 3M Company, Science Research Center, 3M Center, Bldg. 201-1N-34, St. Paul, MN 55144.
‡Present address: Essilor of America, Inc., Optical Thermoplastics R&D, St. Petersburg, FL 33709.

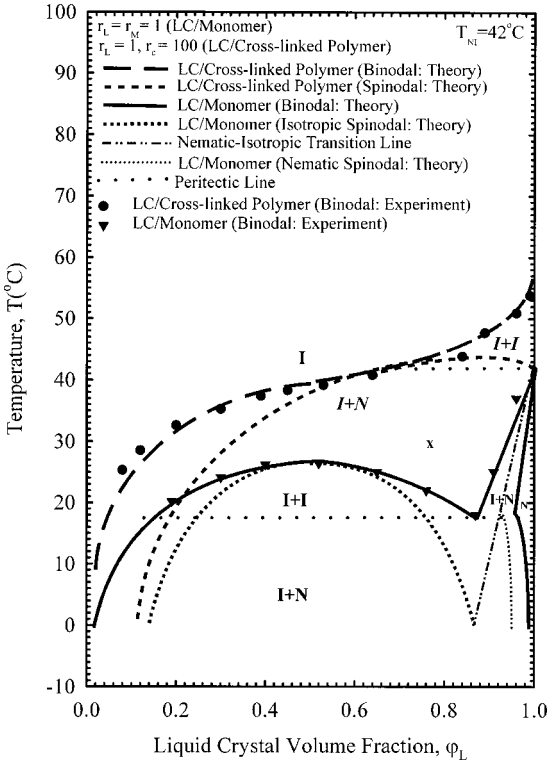

FIG. 1. Calculated coexistence and spinodal curves of mixtures of LC/monomer and LC/cross-linked polymer in comparison with the experimental cloud point phase diagrams of the K21/NOA65 system. The coexistence regions for the LC/network system were labeled with italic letters to distinguish them from those of the LC/monomer blend.

lated by incorporating the local free energies of isotropic mixing, nematic ordering, and network elasticity into the time-dependent Ginzburg-Landau equations (TDGL model *C*) [14,15] in conjunction with the photopolymerization kinetics. It is of particular interest that our simulated results qualitatively capture the experimental H-PDLC morphology reported by Bunning and co-workers [3–8].

II. THEORETICAL MODEL

A. Description of pattern photopolymerization of LC/monomer mixture

Let us consider a binary mixture of nematic LC and multifunctional monomer that exhibits an upper critical solution temperature (UCST) phase diagram overlapping with the nematic-isotropic transition of the constituent LC (see Fig. 1). Polymerization is triggered isothermally in the isotropic state by allowing two propagating UV laser beams to interfere at a certain angle (see Fig. 2). Photopolymerization of monomer occurs preferentially in the high intensity regions relative to that in the low intensity regions. As a consequence, a concentration gradient develops in the mixtures, which allows LC molecules to diffuse from a high intensity to a low intensity region, whereas monomer molecules diffuse in the opposite direction, thereby forming LC-rich layers alternating periodically with polymer-rich layers (Fig. 2).

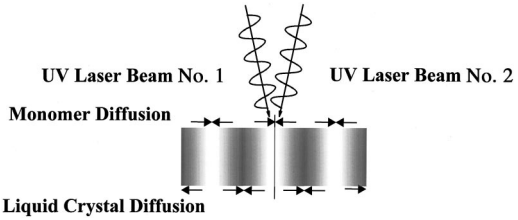

FIG. 2. Schematic illustration of periodic fringes formed by mixing of two UV waves, showing constructive and destructive interference. During photopolymerization, monomers diffuse toward the bright region where the reaction rate is the highest, and, vice versa, the LC molecules diffuse into the dark region where the reaction rate is minimum.

In previous papers [11–13], we have investigated theoretically and experimentally the dynamics of photopolymerization-induced phase separation in mixtures of a low molar mass nematic LC and a multifunctional monomer subjected to uniform UV irradiation. For pattern photopolymerization one must account for the spatial variation of the reaction rate induced by the periodic UV intensity (Fig. 2).

Consider a H-PDLC film in the form of a square grid of length L. Let N be the number of periodic layers (i.e., inversely proportional to layer thickness); then the intensity of radiation I may be described as

$$I = I_0 \cos^2\left(\frac{xN}{L}\pi\right), \tag{1}$$

where I_0 is the maximum intensity, while x is the distance measured along the horizontal axis. Since the rate of photopolymerization $d\alpha/dt'$ is proportional to the square root of the incident intensity, i.e., $d\alpha/dt' \propto I^{1/2}$, one may write

$$\frac{d\alpha}{dt'} = k' I_0^{1/2} \cos\left(\frac{xN}{L}\pi\right)(1-\alpha), \tag{2}$$

where t is time, α represents fractional conversion of monomer to polymer, and k' is the apparent reaction constant in units of reciprocal time. I_0 is the intensity of incident radiation, which was accounted for through the reaction constant during the simulation. For a fixed N and L, x is the variable that determines the regions where the photoreaction rate varies periodically. In the simulation, the reaction time t' and the reaction kinetic coefficient k' may be renormalized in dimensionless units as $t=(\Lambda/l^2)t'$, $k=(l^2/\Lambda)k'$, where Λ is the mutual diffusion coefficient and l is the characteristic length scale. When $N=0$, Eq. (2) reduces to that of the uniform illumination case (see Ref. [13]).

B. Description of dynamics of phase separation and pattern formation

The model proposed here is based on coupled time-dependent Ginzburg-Landau equations, known as model *C*, which consists of conserved concentration and nonconserved orientational order parameters [14,15]. Model *C* has been successfully applied to the elucidation of dynamics of phase

separation and pattern formation in thermal-quench-induced phase separation of liquid-crystal polymer solutions [16,17] and LC/linear polymer mixtures [18–22]. Recently, model *C* has been coupled with the reaction kinetics to describe the photopolymerization-induced phase separation dynamics of LC/polymer mixtures subjected to uniform irradiation [13].

We extend the same methodology to describe the dynamics of pattern polymerization-induced phase separation in H-PDLC films. In view of the fast nature of photopolymerization, it is reasonable to assume that the conversion of monomer to polymer is almost instantaneous; residual monomer, if any, is considered to be miscible with the emerging polymer. Treating the system as pseudo-two-phase, the reaction kinetics of the pattern photopolymerization [Eq. (3)] may be coupled with the TDGL model *C* equations [Eqs. (4) and (5)] by incorporating the free energies of isotropic mixing, nematic ordering, and network elasticity as follows [14,15]:

$$\frac{\partial \varphi_M}{\partial t} = \nabla \cdot \left[\Lambda \nabla \frac{\delta F}{\delta \varphi_M} \right] + \eta_{\varphi_M} \quad \text{or}$$

$$\frac{\partial \varphi_P}{\partial t} = \nabla \cdot \left[\Lambda \nabla \frac{\delta F}{\delta \varphi_P} \right] + \eta_{\varphi_P}, \tag{3}$$

$$\frac{\partial \varphi_L(r,t)}{\partial t} = \nabla \cdot \left[\Lambda \nabla \left(\frac{\delta G}{\delta \varphi_L} \right) \right] + \eta_{\varphi}, \tag{4}$$

$$\frac{\partial s(r,t)}{\partial t} = -R \left(\frac{\delta G}{\delta s} \right) + \eta_s, \tag{5}$$

where $\varphi_L(r,t)$ is the conserved concentration order parameter (or volume fraction) of the LC at position r and dimensionless time t, whereas $s(r,t)$ is the nonconserved orientational order parameter of the LC at the same location and time. Note that the orientational order parameter $s(r,t)$ is treated as scalar for simplicity. A general and more complete approach would be to treat it as a tensor form (e.g., see Refs. [18] and [19]). If the monomer and polymer are immiscible, it is necessary to solve three coupled equations, i.e., Eqs. (3)–(5); otherwise, only two coupled equations would be adequate, e.g., Eq. (5) with Eq. (3) or with Eq. (4). We chose Eqs. (4) and (5) in the simulation under the assumption that the monomers and the emerging polymer are miscible. Furthermore, the monomer $\varphi_M(r,t)$ and the emerging polymer $\varphi_P(r,t)$ concentrations are related to $\varphi_L(r,t)$ via the fractional conversion α as follows [13]

$$\varphi_M = (1-\alpha)(1-\varphi_L) \quad \text{or} \quad \varphi_P = \alpha(1-\varphi_L). \tag{6}$$

As polymerization is initiated, some of the monomer is converted to polymer; thus the system is composed of LC, monomer, and polymer. The incompressibility condition gives $\varphi_L + \varphi_P + \varphi_M = 1$. The quantity Λ in Eq. (3) is the mutual diffusion coefficient having the property of Onsager reciprocity [23]

$$\Lambda = \frac{\Lambda_L \Lambda_M + \Lambda_L \Lambda_P + \Lambda_M \Lambda_P}{\Lambda_L + \Lambda_M + \Lambda_P}, \tag{7}$$

where $\Lambda_L = \varphi_L r_L D_L$, $\Lambda_M = \varphi_M r_M D_M$, and $\Lambda_P = \varphi_P r_P D_P$. D_L, D_M, and D_P are the self-diffusion coefficients of LC, monomer, and polymer, respectively, while r_L, r_M, and r_P are their respective segment lengths. Since the self-diffusion coefficient of the polymer is inversely proportional to the square of the number of segments ($D_P \propto 1/r_P^2$), and $r = \infty$ for a cross-linked polymer, it follows that $D_P = 0$. Thus $\Lambda_P = 0$.

The coefficient R in Eq. (5) is related to the rotational mobility of the LC molecules, and is taken as constant for simplicity [16], while the quantities η_φ and η_s are thermal noise in the concentration and orientation fields, respectively, satisfying the fluctuation dissipation theorem. Since s is coupled to φ, it follows that η_s is also coupled to η_φ. The total free energy of the system, G, may be written as [14]

$$G = \int_v [g(\varphi_L, \varphi_M, \varphi_P, s) + \kappa_\varphi |\nabla \varphi_L|^2 + \kappa_s |\nabla s|^2] dv \tag{8}$$

where $g(\varphi_L, \varphi_M, \varphi_P, s)$ is the local free energy density of the system. The terms $\kappa_\varphi |\nabla \varphi_L|^2$ and $\kappa_s |\nabla s|^2$ are nonlocal terms associated with the gradients of the LC concentration and orientational order parameters, respectively. κ_φ and κ_s are the coefficients of the corresponding interface gradients, which are taken as constants for simplicity. The local free energy density of the mixture, g, consists of isotropic mixing g^i, nematic ordering g^n, and elasticity g^e free energy densities. The free energy density of isotropic mixing may be described in the context of the Flory-Huggins theory [24,25] as extended to a three-component system in what follows [23]:

$$g^i = \frac{\varphi_L \ln \varphi_L}{r_L} + \frac{\varphi_M \ln \varphi_M}{r_M} + \frac{\varphi_P \ln \varphi_P}{r_P} + (\chi_{LM} \varphi_L \varphi_M + \chi_{LP} \varphi_L \varphi_P + \chi_{MP} \varphi_M \varphi_P). \tag{9}$$

Since residual monomers and the emerging polymers are assumed to be miscible, it is reasonable to regard χ_{MP} as zero or negligibly small relative to the other interaction parameters. Therefore, we take $\chi_{LM} = \chi_{LP} = \chi$. Since for a cross-linked polymer $r_P = \infty$, and $r_L = r_M = 1$ for LC and monomer molecules, Eq. (9) reduces to

$$g^i = \varphi_L \ln \varphi_L + \varphi_M \ln \varphi_M + \chi(\varphi_L \varphi_M + \varphi_L \varphi_P). \tag{10}$$

The isotropic interaction parameter χ is taken to be an inverse function of temperature T of the form $\chi = A + (\chi_c - A) T_c / T$, where T_c and χ_c are critical values with reference to the starting LC/monomer system (see Fig. 1), while A is an adjustable parameter to account for the broadness of the coexistence curve. In the context of Maier-Saupe theory [26,27], the nematic ordering free energy density g^n may be expressed as

$$g^n = \frac{1}{r_L} (-\varphi_L \ln z + \tfrac{1}{2} \nu \varphi_L^2 S^2), \tag{11}$$

where z and s are, respectively, the normalized partition function and the nematic order parameter defined by the integrals [21]

$$z=\int_0^1 \exp\left[\frac{\nu\varphi_L s}{2}(3x^2-1)\right]dx, \tag{12}$$

$$s=\frac{3}{2z}\left\{\int_0^1 x^2\exp\left[\frac{\nu\varphi_L s}{2}(3x^2-1)\right]dx-\frac{1}{2}\right\}, \tag{13}$$

where $x=\cos\theta$, while θ is the angle between the nematic LC director and the reference axis. The nematic interaction parameter ν is related to the nematic-isotropic transition temperature T_{NI} as $\nu=4.541(T_{NI}/T)$ [27]. For a flexible cross-linked polymer chain obeying ideal Gaussian chain statistics the elastic free energy g^e may be described as [28]

$$g^e=\frac{2\alpha_e}{2r_c}\Phi_0^{2/3}(\varphi_P^{1/3}-\varphi_P)+\frac{\beta_e}{r_c}\varphi_P\ln\varphi_P, \tag{14}$$

where α_e and β_e are network model parameters and r_c is the segment length between cross-linked points. The Flory affine network model [30] was employed in the calculation assuming the network functionality $f=3$. The parameter Φ_0 in Eq. (14) represents the reference volume fraction of the polymer network, which is taken as the volume fraction at the onset of cross-linking, i.e., $\Phi_0=\varphi_P$ [29]. Taking the variational derivatives of G with respect to φ_L and s according to Eq. (8) and inserting them into Eqs. (4) and (5) gives

$$\frac{\partial\varphi_L}{\partial t}=\boldsymbol{\nabla}\cdot\left[\Lambda\boldsymbol{\nabla}\left(\frac{\partial g^i}{\partial\varphi_L}+\frac{\partial g^n}{\partial\varphi_L}+\frac{\partial g^e}{\partial\varphi_L}-\kappa_\varphi\nabla^2\varphi_L\right)\right]+\eta_\varphi, \tag{15}$$

$$\frac{\partial s}{\partial t}=-R\left(\frac{\partial g^n}{\partial s}-\kappa_s\nabla^2 s\right)+\eta_s, \tag{16}$$

where the partial derivatives appearing on the right hand sides of Eqs. (15) and (16) may be obtained [13,21] from Eqs. (10), (11), and (14).

C. Numerical simulation procedure

To simulate the spatiotemporal growth of PIPS in H-PDLC, Eqs. (15) and (16) were solved numerically using a finite difference method on a 128×128 square grid based on specified initial and boundary conditions. For spatial steps, a central difference discretization scheme was used, while a forward difference discretization was utilized for temporal steps. Both the grid size and the time step were chosen sufficiently small to ensure that changes in them exerted little or no effect on the calculated results. The periodic boundary conditions used were similar to those of previously reported work [16,21]. In the simulations, photopolymerization was initiated in the isotropic region of the starting LC/monomer phase diagram (see Fig. 1). The initial LC volume fractions $\varphi_L(r,0)$ at each grid point were calculated by triggering random thermal noise that satisfied the fluctuation-dissipation theorem. Using known $\varphi_L(r,0)$, the initial $s(r,0)$ was obtained through the self-consistent solution of Eqs. (14) and (15). The values of Λ, R, κ_L, and κ_s used in this work are within the range employed by others [16,20]. Fourier transformation was also undertaken on the emerging patterns in the concentration and order parameter fields.

III. RESULTS AND DISCUSSION

A. Phase diagrams of LC/monomer and LC/cross-linked polymer network

Figure 1 shows the calculated binodal and spinodal curves of the LC/monomer and the LC/cross-linked polymer systems in comparison with the experimental cloud point phase diagram of a reference system. For detailed calculations and experimental procedures, interested readers are referred to our previous paper [31]. Here, we shall briefly discuss the effect of cross linking on the phase diagram based on the binodal curve that separates the stable (one-phase) from the unstable (two-phase) regions. As evident in Fig. 1, the LC/monomer coexistence curve is a UCST type overlapping with the nematic-isotropic transition of the constituent LC. The LC/monomer phase diagram is similar in shape to that of the LC/linear polymer mixture [27,32], except that the critical point of the starting LC/monomer system is located at ($\varphi_L=0.5$) due to the comparable size of the constituent molecules.

Photopolymerization was carried out on a typical mixture ($\varphi_L=0.75$) in the isotropic region of the starting LC/monomer as indicated by $\times$ in Fig. 1. As polymerization advances, the binodal curve moves upward asymmetrically toward the higher LC content side. When it crosses the reaction temperature (point $\times$), the system becomes unstable and undergoes phase separation. The process of phase separation is influenced by the network elasticity; hence for the LC/cross-linked polymer the coexistence curve makes an upward turn asymptotically near the pure LC axis. There appears to be no identifiable critical point in the binodal curve of the LC/cross-linked polymer system. Bauer, Briber, and Han [29] made a similar observation in the case of blends of linear polymer/cross-linked network. Since the polymer network can no longer dissolve in the pure LC, the equilibrium phases are pure LC solvent and swollen network (or gel). It should be noted that in calculating the LC/cross-linked polymer phase diagram the LC ordering free energy is not affected by the polymer topology [31].

B. Dynamics of uniform photopolymerization-induced phase separation

Prior to examining the stripe pattern formation during PIPS, it is instructive to examine the PIPS dynamics arising from uniform UV irradiation. Numerical simulation was conducted on a LC/monomer mixture with the following conditions: $N=0$, $L=128$, $\varphi_L=0.75$, $T=30\,^\circ$C, $I_0=1$, and $k=10^{-4}$. The polymerization temperature corresponds to the isotropic state of the LC/monomer mixture (see Fig. 1). Figure 3 exhibits the dimensionless time sequence of (a) the emergence of LC domains and (b) the corresponding Fourier transform scattering images during the course of phase separation. Note that the gray level of the images was normalized for the sake of clarity. The initial morphological pictures are representative of random thermal fluctuations. With elapse of time, interconnected structures emerge in the concentration field. The pattern in the orientation field lags behind, as LC molecules have to segregate out before nematic ordering can

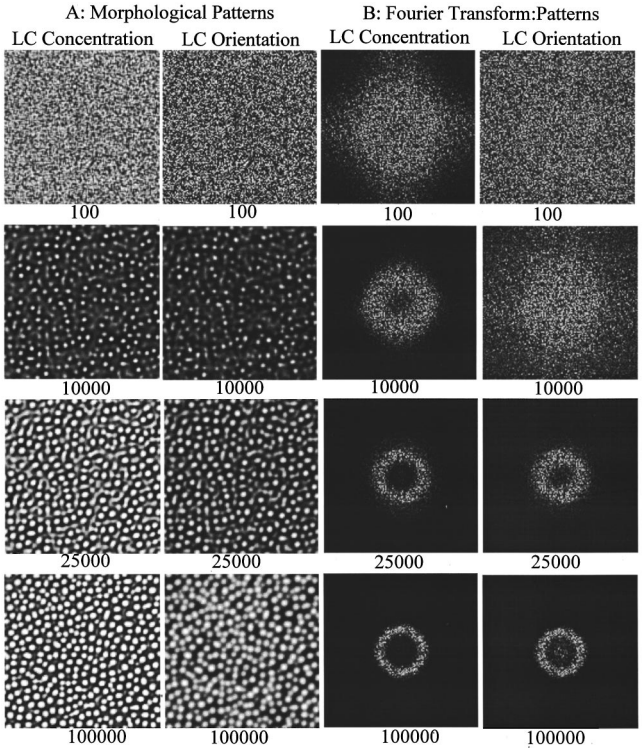

FIG. 3. Spatiotemporal evolution of simulated morphology and Fourier transform patterns of a standard PDLC formed during uniform UV irradiation. Simulation was performed using $\varphi_L = 0.75$, $T = 30\,^{\circ}\mathrm{C}$, and $k = 10^{-4}$. The indicated time steps are in dimensionless units.

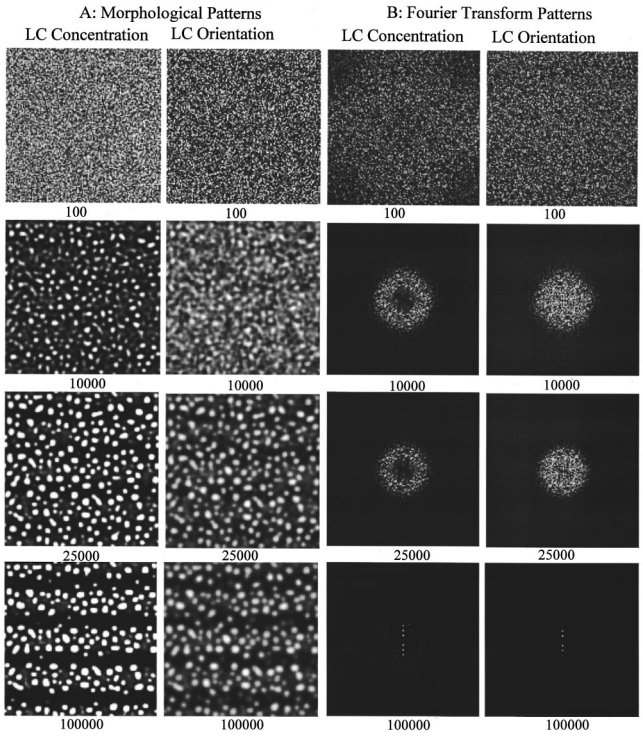

FIG. 4. Spatiotemporal evolution of simulated morphology and Fourier transform patterns of a H-PDLC formed during pattern photopolymerization. Simulation was performed with the following parameters: $\varphi_L = 0.75$, $T = 30\,^{\circ}\mathrm{C}$, $k = 10^{-4}$, $N = 4$, and $L = 128$ in dimensionless units.

take place. The interconnected structures grow in time and then break down into droplets. With continued elapsed time, the domains increase in size, but the network formation seemingly prevents further coalescence. At late stages, however, the two order parameter fields appear to merge to the same spatial topology.

As shown in Fig. 3(b), the initial scattering patterns are very diffuse and weak. It is seen that the initial scattering patterns in the orientation order parameter field lag behind those of the concentration field. As time elapses, the scattering patterns intensify and transform to halos, while collapsing to smaller diameters. The appearance of sharp scattering halos implies the development of domain periodicity, whereas the collapse of the halos to smaller diameters may be attributed to the domain growth. Later both fields evolve to the same scattering halo, which is consistent with the results of Fig. 3(a).

C. Dynamics of stratified pattern formation via periodic photopolymerization-induced phase separation

Next, we examine the emergence of stratified pattern formation. The simulation was performed on a LC/monomer mixture of the same composition under the same conditions as that in Fig. 3, except that $N = 4$ and $L = 128$. Figure 4 shows snapshots of (a) spatiotemporal evolution of morphologies (first two columns) and (b) the corresponding Fourier transform patterns (last two columns) for both the concentration and orientation order parameters. With the progression of time, LC droplets emerge (e.g., see 10^3 time steps). By virtue of the stratified pattern polymerization, i.e., the periodic spatial modulation of the reaction and hence of phase separation, the LC droplets formed are confined in discrete layers alternating periodically with polymer-rich layers (dark regions). It should be pointed out that only the LC molecule and monomer are permitted to diffuse in the simulation as the emerging polymer chains are chemically fixed due to network formation. The LC domains grow through coalescence within the confined layers. These simulated patterns are in good accord with the experimental H-PDLC morphologies reported by Bunning and co-workers [5–8].

Regarding a rough estimation of the droplet size, it depends on the choice of the length scale, the characteristic time, and the mutual diffusion coefficient. If one utilizes an average diffusivity of $10^{-6}\,\mathrm{cm}^2/\mathrm{s}$ (for the monomer and a low molecular weight LC), a characteristic time of $10^{-6}\,\mathrm{s}$, and assuming that the photopolymerization time is very fast, say 1 s, the estimated characteristic size would be of the order of 33 nm. Hence, the calculated picture frame (128×128) would be approximately 4.2 $\mu\mathrm{m}^2$. This in turn gives an average droplet size of about 330 nm. These estimated length scales are within the range reported by Bunning *et al.* [5–8].

As shown in Fig. 4(b), the corresponding Fourier transform patterns are very diffuse and weak initially. Scattering rings emerge as droplets form. As the droplet domains grow the diameter of the scattering rings gets smaller. Subse-

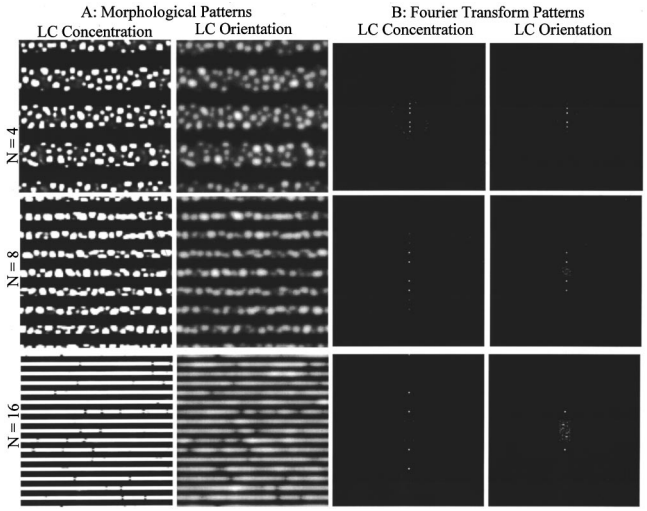

FIG. 5. Effect of thickness of periodic layers on simulated morphological and Fourier transform patterns. The simulation parameters are the same as in Fig. 4, except that here the dimensionless time steps $t=10^5$.

quently, diffraction spots emerge by overlapping with the existing scattering halo. The diffraction spots may be ascribed to the development of periodic layers in the concentration field, whereas the weak surrounding scattering halo may be attributed to scattering arising from the interparticle interference of the droplets within the layers. To improve the diffraction performance of a H-PDLC, the scattering rings should be suppressed or eliminated completely. In other words, the droplet morphology within the layers must be eliminated, which may be achieved by narrowing the layers such that the LC molecules can grow only along the stripes.

Figure 5 shows the simulated patterns for $N=4$, 8, and 16 and their effects on the emerging H-PDLC morphologies and the corresponding Fourier transform images. The simulation parameters are the same as in Fig. 4 except that the calculated patterns are for $t=10^5$ steps. As the number of periodic layers N increases, the layer thickness is reduced accordingly. When the number of layers $N=16$, the layer thickness is so restricted that the LC droplets grow preferentially along the narrow stripes. It is also apparent that the scattering halo resulting from the interparticle interference of the LC droplets disappears.

Figure 6(a) shows the comparison of a one-dimensional scan of the concentration field as a function of the number of layers. At $N=4$, the LC concentration profile is broad and appears heterogeneous due to the presence of the LC domains within the layer. With eight layers, the LC distribution is somewhat improved. At $N=16$, the LC concentration is truly uniform. As shown in Fig. 6(b), the diffracted intensity peaks (or structure factor in dimensionless units peaks) of the $N=16$ case are well resolved as compared to the other two cases, suggesting an improvement in the diffraction efficiency. In addition, the growth dynamics of the domains could be affected by the thickness effect.

In Fig. 7 are shown the temporal growth curves for the $\varphi_L=0.75$ blend for various N values in comparison with that for uniform illumination ($N=0$). In the $N=0$ case, phase

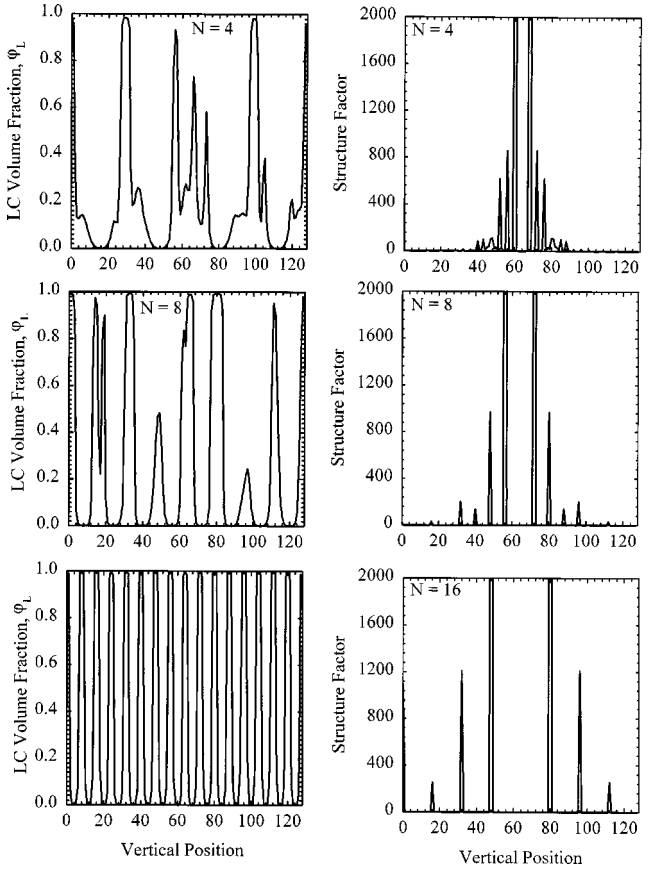

FIG. 6. One-dimensional scans of the concentration profiles and the vertical scan of the diffracted intensity of the corresponding Fourier transform patterns in Fig. 5. Note that the zeroth order Fourier peak was masked in order to discern the higher order, smaller peaks. Both the concentration and structure factor are in dimensionless units.

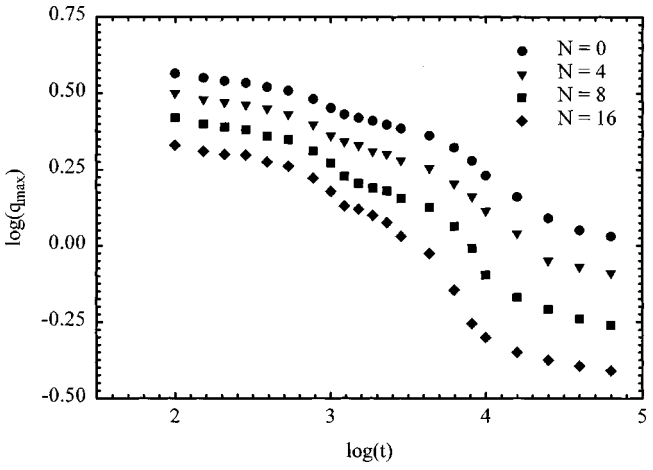

FIG. 7. Comparison of the temporal growth dynamic curves for various N values (inversely proportional to the layer thickness). $N=0$ represents the case of uniform illumination.

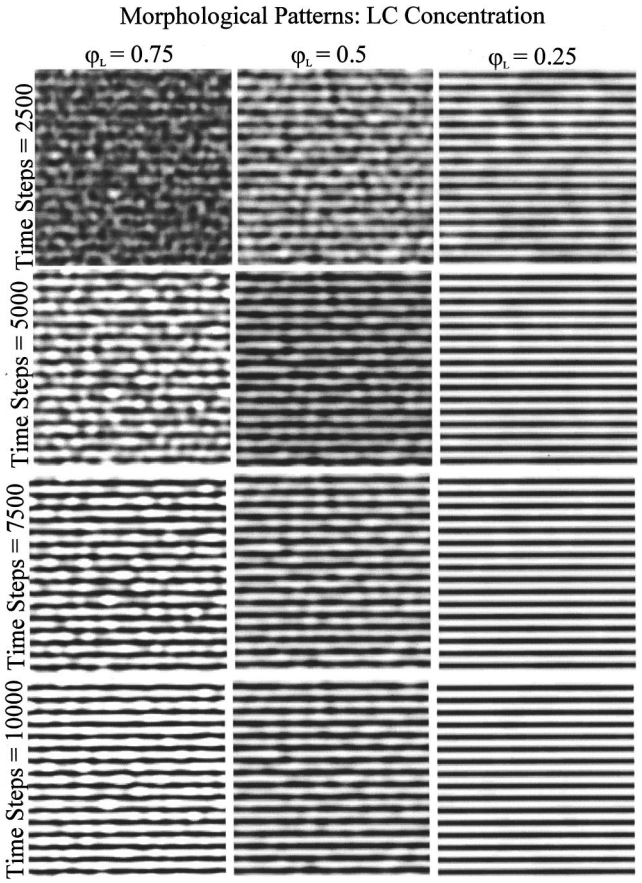

FIG. 8. Spatiotemporal growth of the LC domains within the emerging stripes driven by the pattern polymerization-induced phase separation for three different LC concentrations. The simulation parameters are the same as in Fig. 4, but emphasis is placed on shorter dimensionless time steps up to 10^4 to discern the early stage of preferential coalescence along the stripes.

separation is first noticed in the concentration field; then nematic ordering takes place within the domains. A subtle change in curvature (or an inflection) in the vicinity of 1000 time steps in the growth curve was discerned. This inflection has been attributed to the consequence of competition between the phase separation and the nematic ordering [13,21]. A similar trend was observed for different N values, except that the growth process was expedited with decreasing layer thickness or increasing N. This observation is not surprising in view of the fact that, as the layer thickness is reduced, the growth occurs preferentially along the layer due to the inability to grow in the lateral direction. It is reasonable to infer that the reduction in layer thickness expedites the coalescence process.

Furthermore, it is of interest to investigate the effect of initial LC concentrations ($\varphi_L = 0.75$, 0.5, and 0.25) on stripe pattern formation as depicted in Fig. 8. During photopolymerization, LC molecules diffuse to dark (low intensity) regions, whereas reactive monomers diffuse to the bright (high intensity) regions. As can be seen at 2500 time steps for $\varphi_L = 0.75$, some LC (white color) domains are seemingly present between the successive layers. With elapsed time, these LC domains are merged with those within the LC-rich

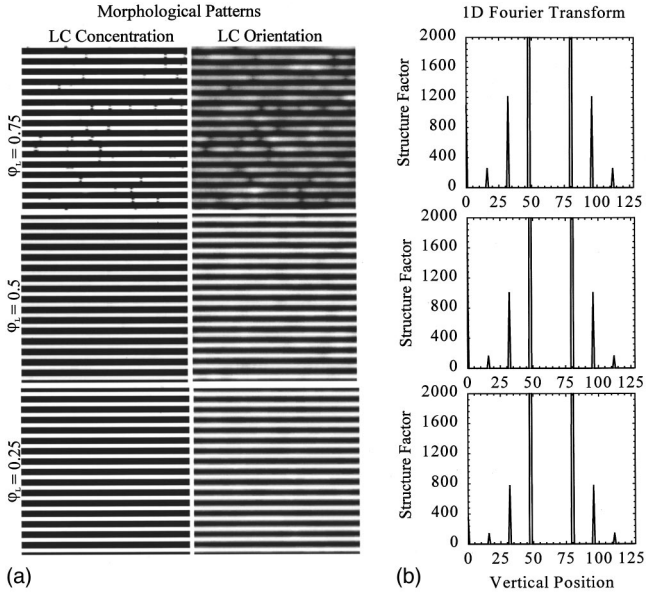

FIG. 9. Effect of LC concentration on the simulated morphologies and the structure factor (diffraction peaks in dimensionless units) of the Fourier transform patterns of the H-PDLC. Note that the zeroth order Fourier peak was masked in order to discern the higher order, smaller peaks. The simulation parameters are the same as in Fig. 8, except for dimensionless time steps $t = 10^5$.

layers. The LC domains grow through coalescence preferentially along the stripes, showing elongated (or interconnected) domains due to confinement by the layer. A similar observation can be made in the case of 50% LC concentration (middle column), except that the emergence of the LC stripes is seemingly faster. The faster domain growth with increasing monomer concentration may be attributed to the faster photopolymerization of the monomer. In the case of very low LC concentration ($\varphi_L = 0.25$), the coalescence process has been greatly expedited due to the fast photopolymerization reaction, and well-aligned LC stripes are exhibited.

As shown in Fig. 9(a), the 75% LC at 10^5 steps has well-aligned stripes in both the concentration and orientational order parameter fields. It should be emphasized that the LC stripes in the 25% and 50% LC compositions are more uniform throughout than those of the 75% LC based H-PDLC films. The diffraction spots remain virtually the same [Fig. 9(b)] for the three compositions. Hence, lowering the LC concentration did not sacrifice the diffraction performance of the H-PDLC. The finding that the LC stripes in the 25% LC are well defined and essentially indistinguishable from those of the 50% and 75% LC content composites suggests that H-PDLC's may be fabricated with lesser amounts of LC, and therefore the cost of materials may be reduced considerably.

IV. CONCLUSIONS

We have demonstrated stripe pattern formation in a holographic polymer-dispersed liquid crystal (H-PDLC) via anisotropic pattern photopolymerization-induced phase separation. The simulated LC droplets are confined in discrete layers alternating periodically with polymer-network-rich

layers. The Fourier transform patterns reveal scattering rings initially, and then show diffraction spots as the periodic layers are formed. As the number of periodic layers is increased, the layer thickness is reduced. The LC droplets grow through coalescing preferentially along the narrow stripes, which in turn gives rise to sharper diffraction spots in the Fourier space. Reducing the LC concentration to 50% or 25% makes the LC directors more uniform throughout the stripes relative to those of 75% LC based H-PDLC films without sacrificing the sharpness of diffraction spots. This observation suggests that H-PDLC's may be fabricated with lesser amounts of LC without sacrificing the diffraction performance.

ACKNOWLEDGMENT

Support of this work by the NSF-STC Center for Advanced Liquid Crystal Optical Materials (ALCOM) via Grant No. 89-20147 is gratefully acknowledged.

[1] P. S. Drzaic, *Liquid Crystal Dispersion* (World Scientific, Singapore, 1995).
[2] J. W. Doane, in *Liquid Crystals: Applications and Uses*, edited by B. Bahadur (World Scientific, Singapore, 1991).
[3] R. L. Sutherland, V. P. Tondiglia, L. V. Natarajan, T. J. Bunning, and W. W. Wade, Appl. Phys. Lett. **64**, 1074 (1994).
[4] V. P. Tondiglia, L. V. Natarajan, R. L. Sutherland, T. J. Bunning, and W. W. Wade, Opt. Lett. **20**, 1325 (1995).
[5] T. J. Bunning, D. L. Vezie, W. W. Adams, L. V. Natarajan, V. P. Tondiglia, and R. L. Sutherland, Polymer **36**, 2699 (1995).
[6] T. J. Bunning, L. V. Natarajan, V. P. Tondiglia, G. Dougherty, and R. L. Sutherland, J. Polym. Sci., Part B: Polym. Phys. **35**, 2825 (1997).
[7] R. T. Pogue, L. V. Natarajan, V. P. Siwecki, T. J. Bunning, V. P. Tondiglia, R. L. Sutherland, and W. W. Adams, Polymer **41**, 733 (2000).
[8] V. Vorflusev and S. Kumar, Science **283**, 1903 (1999).
[9] V. V. Krongauz, E. R. Schmelzer, and R. M. Yohannan, Polymer **32**, 1654 (1991).
[10] X. Y. Wang, Y.-K. Yu, and P. L. Taylor, J. Appl. Phys. **80**, 3285 (1996).
[11] D. Nwabunma, K.-J. Kim, Y. Lin, L.-C. Chien, and T. Kyu, Macromolecules **31**, 6806 (1998).
[12] D. Nwabunma, H.-W. Chiu, and T. Kyu, Macromolecules **33**, 1416 (2000).
[13] D. Nwabunma, H.-W. Chiu, and T. Kyu, J. Chem. Phys. **113**, 6429 (2000).
[14] J. D. Gunton, M. San Miguel, and P. S. Sahni, in *Phase Transition and Critical Phenomena*, edited by C. Domb and J. L. Lebowitz (Academic, New York, 1993).
[15] P. C. Hohenberg and B. I. Halperin, Rev. Mod. Phys. **49**, 435 (1977).
[16] J. R. Dorgan and D. Yan, Macromolecules **31**, 193 (1998).
[17] J. Fukuda, Phys. Rev. E **58**, 6939 (1998); **59**, 3275 (1999).
[18] A. J. Liu and G. Fredrickson, Macromolecules **26**, 2817 (1993).
[19] A. M. Lapena, S. C. Glotzer, S. A. Langer, and A. J. Liu, Phys. Rev. E **60**, 29 (1999).
[20] Z. Lin, H. Zhang, and Y. Yang, Macromol. Theory Simul. **6**, 1153 (1997); Macromol. Chem. Phys. **200**, 943 (1999).
[21] H.-W. Chiu and T. Kyu, J. Chem. Phys. **110**, 5998 (1999).
[22] A. Matsuyama, R. M. L. Evans, and M. E. Coates, Phys. Rev. E **61**, 2977 (2000).
[23] M. Takenaka and T. Hashimoto, Phys. Rev. E **48**, R647 (1993).
[24] P. J. Flory, J. Chem. Phys. **10**, 51 (1942).
[25] M. L. Huggins, J. Chem. Phys. **9**, 440 (1941).
[26] M. Maier and A. Saupe, Z. Naturforsch. A **13**, 564 (1958); **14**, 882 (1959); **15**, 287 (1960).
[27] C. Shen and T. Kyu, J. Chem. Phys. **103**, 7471 (1995).
[28] K. Dusek, J. Polym. Sci., Part C: Polym. Symp. **16**, 1289 (1967).
[29] B. J. Bauer, R. M. Briber, and C. C. Han, Macromolecules **22**, 940 (1989).
[30] P. J. Flory, J. Chem. Phys. **18**, 108 (1950).
[31] D. Nwabunma and T. Kyu, Macromolecules **32**, 664 (1999).
[32] Y. Yang, J. Lu, H. Zhang, and T. Yu, Polym. J. (Tokyo) **26**, 880 (1994).